fractal and fractional

MDPI

Article

Newly Developed Analytical Scheme and Its Applications to the Some Nonlinear Partial Differential Equations with the Conformable Derivative

Li Yan [1], Gulnur Yel [2], Ajay Kumar [3], Haci Mehmet Baskonus [4,*] and Wei Gao [5]

[1] School of Engineering, Honghe University, Mengzi 661199, China; yanli@uoh.edu.cn
[2] Department of Education, Final International University, Kyrenia 99370, Mersin 10, Turkey; gulnuryel33@gmail.com
[3] Department of Science and Technology, Bakhtiyarpur College of Engineering, Champapur, Dedaur, Bakhtiyarpur 803212, India; kajay9249@gmail.com
[4] Faculty of Education, Harran University, Sanliurfa 63050, Turkey
[5] School of Information Science and Technology, Yunnan Normal University, Kunming 650500, China; gaowei@ynnu.edu.cn
* Correspondence: hmbaskonus@gmail.com

Abstract: This paper presents a novel and general analytical approach: the rational sine-Gordon expansion method and its applications to the nonlinear Gardner and (3+1)-dimensional mKdV-ZK equations including a conformable operator. Some trigonometric, periodic, hyperbolic and rational function solutions are extracted. Physical meanings of these solutions are also presented. After choosing suitable values of the parameters in the results, some simulations are plotted. Strain conditions for valid solutions are also reported in detail.

Keywords: nonlinear Gardner and (3+1)-dimensional mKdV-ZK equations; conformable operator; RSGEM; periodic wave; hyperbolic solutions; complex hyperbolic; mixed complex hyperbolic solutions

Citation: Yan, L.; Yel, G.; Kumar, A.; Baskonus, H.M.; Gao, W. Newly Developed Analytical Scheme and Its Applications to the Some Nonlinear Partial Differential Equations with the Conformable Derivative. *Fractal Fract.* **2021**, *5*, 238. https://doi.org/10.3390/fractalfract5040238

Academic Editor: Stanislaw Migorski

Received: 2 September 2021
Accepted: 18 November 2021
Published: 23 November 2021

1. Introduction

Fractional calculus appeared in the middle of the 17th century. However, it is now attracting substantial interest from scientists due to its applications in many fields [1–6]. Many researchers have directed their studies to fractional calculus. Several different definitions of fractional operators have been presented in the literature since the middle of the 17th century. These operators play an important role in understanding the characteristic properties of real-world problems. One of the most significant operators of the fractional derivatives is the Caputo operator [7,8]. This operator satisfies the basic rules of classical calculus. In this regard, Brzezinski presented the comparisons of fractional definitions [9]. Youssef and his team applied the Haar wavelet to extract the solutions of Poisson's Equation in [10]. Eslami and his team observed the general features of the Wu–Zhang system, including a conformable operator [11]. The fundamental properties of hepatitis E virus were observed via the Caputo–Fabrizio operator in [12]. Many important models and their deep properties were investigated by using a conformable operator in [13–32].

In this paper, firstly, we consider the nonlinear Gardner equation containing a conformable operator in the following form [33–37]:

$$u_t^{\gamma}(x,t)+6[u(x,t)-\lambda^2 u(x,t)^2]u_x(x,t)+u_{xxx}(x,t)=0,\ \ t\geq 0,\ \ 0<\gamma\leq 1, \tag{1}$$

where λ is a nonzero real number, $u(x,t)$ is a dependent function of x and t, the terms uu_x and u^2u_x are used to represent the nonlinear wave, and u_{xxx} is used to explain the spreading of waves. Equation (1), formed by combining KdV and mKdV equations, is used to describe the interior shallow water solitary waves.

Secondly, the nonlinear (3+1)-dimensional mKdV-ZKE containing a conformable operator given by [38]

$$u_t^{\gamma}(x,y,z,t)+pu(x,y,z,t)^2u_x(x,y,z,t)+u_{xxx}(x,y,z,t)+u_{xyy}(x,y,z,t)+u_{zzx}(x,y,z,t)=0, \tag{2}$$

is studied. In Equation (2), $t>0, \quad 0<\gamma\leq 1$ and also p is a nonzero real number. $u(x,y,z,t)$ is a dependent function of x,y,z and t, the term u^2u_x is used to represent the nonlinear waves, and u_{xxx} is used to explain the spreading of waves.

The rest of the paper is organized as follows. In Section 2, we give some definitions and theorems related to the conformable operator. In Section 3, we present the general properties of the rational sine-Gordon expansion method (RSGEM). In Section 4, we apply the RSGEM to the nonlinear Gardner and (3+1)-dimensional mKdV-ZK equations including a conformable operator to obtain analytical solutions such as periodic, singular, trigonometric, and traveling solutions. Section 5 contains the discussion and physical meanings of the results reported in this paper. Finally, we present a conclusion along with ideas about future work regarding this framework in Section 6.

2. General Properties of Conformable Operator

This section presents the definition and theorem about the conformable operator as follows [7].

Definition 1. *Given a function $f:[0,\infty)\longrightarrow R$, then the conformable operator definition of $f(t)$ order α is defined as*

$$T_{\alpha}(f)(t)=\lim_{\varepsilon\to 0}\frac{f(t+\varepsilon t^{1-\alpha})-f(t)}{\varepsilon}$$

for all $t>0$, $\alpha\in(0,1)$. If f is α-differentiable in $(0,a), a>0$, and $\lim_{t\to 0^+}f^{(\alpha)}(t)$ exists, then we define
$f^{(\alpha)}(0)=\lim_{t\to 0^+}f^{(\alpha)}(t)$.

A conformable operator satisfies some properties given in the following theorem.

Theorem 1. *Let $\beta\in(0,1]$ and f,g be β-differentiable at point $t>0$. Then,*
(1) $T_{\beta}(af+bg)=aT_{\beta}(f)+bT_{\beta}(g)$, for all $a,b\in R$;
(2) $T_{\beta}(t^p)=pt^{p-\beta}$ foll all $p\in R$;
(3) $T_{\beta}(\chi)=0$, for all constant functions $f(t)=\chi$;
(4) $T_{\beta}(fg)=fT_{\beta}(g)+gT_{\beta}(f)$;
(5) $T_{\beta}(\frac{f}{g})=\frac{gT_{\beta}(f)-fT_{\beta}(g)}{g^2}$;
(6) If f is differentiable, then $T_{\beta}(f)(t)=t^{1-\beta}\frac{df(t)}{dt}$.

3. General Properties of RSGEM

In this section, we introduce the general properties of RSGEM. Before presenting the RSGEM based on the sine-Gordon equation, we need to investigate the sine-Gordon equation.

3.1. The Sine-Gordon Equation

The sine-Gordon equation is given by [39–41]

$$u_{xx}-u_{tt}=m^2\sin(u), \tag{3}$$

where $u=u(x,t)$, m is a nonzero real number. Applying the wave transformation given as $u=u(x,t)=U(\xi),\xi=\mu(x-ct)$ to Equation (3) yields

$$U''=\frac{m^2}{\mu^2(1-c^2)}\sin(U), \tag{4}$$

where $U = U(\xi)$, $U'' = \frac{d^2U}{d\xi^2}$, and c is the velocity of the wave. After some calculations, we obtain

$$(\frac{U'}{2})^2 = \frac{m^2}{\mu^2(1-c^2)} \sin^2(\frac{U}{2}) + r, \tag{5}$$

where r is an integral constant and a nonzero real number. Taking $r = 0$, $w(\xi) = \frac{U(\xi)}{2}$ and $a^2 = \frac{m^2}{\mu^2(1-c^2)}$, Equation (5) becomes

$$w' = a\sin(w). \tag{6}$$

In (6), if $a = 1$, we reach

$$w' = \sin(w). \tag{7}$$

Solving (7) by using the separating variable method

$$\frac{dw}{d\xi} = \sin(w) \Rightarrow \frac{1}{\sin(w)}dw = d\xi,$$

we obtain the following two important properties:

$$\sin(w) = \sin(w(\xi)) = \frac{2pe^{\xi}}{p^2e^{2\xi}+1} \mid p_{=1} = \operatorname{sech}(\xi), \tag{8}$$

$$\cos(w) = \cos(w(\xi)) = \frac{p^2e^{2\xi}-1}{p^2e^{2\xi}+1} \mid p_{=1} = \tanh(\xi). \tag{9}$$

where p is a nonzero real number.

3.2. The RSGEM

RSGEM is the generalized version of the sine-Gordon expansion method (SGEM). Let us consider the nonlinear partial differential equation given by

$$P(u, u_x, u_t, u_{xx}, u_{tt}, u^2, \cdots) = 0. \tag{10}$$

If we apply $u = u(x,t) = U(\xi), \xi = \mu(x - ct)$ into Equation (10), we get the following nonlinear ordinary differential equation (NODE):

$$N(U, U', U'', U^2, \cdots) = 0, \tag{11}$$

where $U = U(\xi)$, $U' = \frac{dU}{d\xi}$, $U'' = \frac{d^2U}{d\xi^2}$. The test function of solution formula for Equation (11) is considered as [42]

$$U(\xi) = \frac{\sum_{i=1}^{n} \tanh^{i-1}(\xi)[A_i\operatorname{sech}(\xi) + C_i\tanh(\xi)] + A_0}{\sum_{j=1}^{m} \tanh^{j-1}(\xi)[B_j\operatorname{sech}(\xi) + D_j\tanh(\xi)] + B_0}. \tag{12}$$

Integrating Equations (8) and (9) into Equation (12), it can be rewritten in the following form:

$$U(w) = \frac{\sum_{i=1}^{n} \cos^{i-1}(w)[A_i\sin(w) + C_i\cos(w)] + A_0}{\sum_{j=1}^{m} \cos^{j-1}(w)[B_j\sin(w) + D_j\cos(w)] + B_0}, \tag{13}$$

where $A_0, A_i, C_i, B_0, B_j, D_j$ are nonzero real numbers to be determined later. It is known that the rational functions are more general than normal polynomial functions with SGEM. If we consider the solution function as the rational function, this means that we have one more parameter. This parameter produces more different solutions to the model studied. Putting Equation (13) into Equation (11), we can obtain the values of $\lambda, \mu, A_0, A_i, C_i, B_0, B_j, D_j$. When we integrate these values of parameters into Equation (12), we find the solutions of Equation (10).

4. Applications of RSGEM

This part applies the RSGEM to the Equations (1) and (2) to obtain some traveling wave solutions such as periodic, trigonometric, traveling, complex and hyperbolic solutions.

4.1. RSGEM to the Gardner Equation Including a Conformable Operator

Considering the wave transformation formula given as

$$u(x,t) = U(\xi), \;\; \xi = \alpha x - \frac{\kappa}{\gamma} t^{\gamma}, \tag{14}$$

where α and κ are nonzero real numbers, we convert Equation (1) into NODE given by

$$\alpha^3 U''' - \kappa U' + 3\alpha (U^2)' - 2\alpha \lambda^2 (U^3)' = 0. \tag{15}$$

Integrating (15) with respect to ξ yields

$$\alpha^3 U'' - \kappa U + 3\alpha U^2 - 2\alpha \lambda^2 U^3 = 0. \tag{16}$$

In (16), the integral constant is zero. Especially, if we take $n = m$ in (13), by the balance principle, we have

$$U(w) = \frac{A_1 \sin(w) + C_1 \cos(w) + A_0}{B_1 \sin(w) + D_1 \cos(w) + B_0}. \tag{17}$$

where $A_1 \neq B_1, C_1 \neq D_1, A_0 \neq B_0$ in the same time. Substituting (17) into (16), the following solutions are obtained.

Case 1. If $A_0 = -C_1,\; B_0 = -\frac{2C_1}{\alpha^2} + D_1,\; B_1 = \frac{A_1^2 + C_1^2 - \alpha^2 C_1 D_1}{\alpha^2 A_1},\; \lambda = \frac{1}{\alpha},\; \kappa = \alpha^3$, we get

$$u_1(x,t) = \frac{\alpha^2 A_1}{A_1 + (-C_1 + \alpha^2 D_1) e^{\alpha x - \frac{t^{\gamma}}{\gamma} \alpha^3}}. \tag{18}$$

Figure 1 shows 3D and 2D graphs of (18) under the suitable values of parameters.

Case 2. When $A_1 = 0,\; A_0 = -C_1,\; B_0 = -\frac{C_1}{2\alpha^2} + D_1,\; B_1 = 0,\; \lambda = -\frac{\sqrt{-\frac{C_1}{\alpha^2} + 4D_1}}{2\sqrt{-C_1 + 4\alpha^2 D_1}}$ and $\kappa = 4\alpha^3$, it gives

$$u_2(x,t) = \frac{-C_1 + C_1 \tanh(\alpha x - \frac{4t^{\gamma}}{\gamma}\alpha^3)}{\frac{-C_1}{2\alpha^2} + D_1 + D_1 \tanh(\alpha x - \frac{4\alpha^3}{\gamma} t^{\gamma})}. \tag{19}$$

Figure 2 presents 3D and 2D graphs of (19) under the suitable values of parameters.

Case 3. Taken as $A_1 = -\frac{i\sqrt{2}\sqrt{\alpha^6 + \alpha^3\kappa - 2\kappa^2}\sqrt{B_0^2 - D_1^2}}{3\alpha}, C_1 = \frac{D_1}{3\alpha}(\alpha^3 + 2\kappa),\; A_0 = \frac{(\alpha^3 + 2\kappa)B_0}{3\alpha}$, $B_1 = \frac{i(\alpha^3 + 2\kappa)\sqrt{\alpha^6 + \alpha^3\kappa - 2\kappa^2}\sqrt{B_0^2 - D_1^2} - 3\sqrt{-\alpha^6(\alpha^6 + \alpha^3\kappa - 2\kappa^2)(B_0^2 - D_1^2)}}{\sqrt{2}(\alpha^6 + \alpha^3\kappa - 2\kappa^2)}$, $\lambda = -\frac{3\sqrt{\alpha(\alpha^3 + \kappa)}}{\sqrt{2}\sqrt{(\alpha^3 + 2\kappa)^2}}$, we obtain

$$u_3(x,t) = \frac{\frac{\tau B_0}{3\alpha} - \frac{i\sqrt{2}\sqrt{\alpha^6 + \alpha^3\kappa - 2\kappa^2}\sqrt{B_0^2 - D_1^2}}{3\alpha}\operatorname{sech}(\alpha x - \frac{t^{\gamma}}{\gamma}\kappa) + \frac{\tau D_1}{3\alpha}\tanh(\alpha x - \frac{t^{\gamma}}{\gamma}\kappa)}{B_0 + \frac{\operatorname{sech}(\alpha x - \frac{t^{\gamma}}{\gamma}\kappa)(i\tau\chi - 3\sqrt{-\alpha^6\chi(B_0^2 - D_1^2)})}{\sqrt{2}(\alpha^6 + \alpha^3\kappa - 2\kappa^2)} + D_1 \tanh(\alpha x - \frac{\kappa}{\gamma} t^{\gamma})}, \tag{20}$$

where $\tau = \alpha^3 + 2\kappa, \chi = \sqrt{\alpha^6 + \alpha^3\kappa - 2\kappa^2}\sqrt{B_0^2 - D_0^1}$. We plot the several graphs of (20) as Figures 3–5.

Case 4. Considering $A_0 = C_1,\; B_0 = \frac{2C_1}{\alpha^2} - D_1,\; B_1 = \frac{A_1^2 + C_1^2 - \alpha^2 C_1 D_1}{\alpha^2 A_1},\; \lambda = -\frac{\sqrt{-C_1 + \alpha^2 D_1}}{\sqrt{-\alpha^2 C_1 + \alpha^4 D_1}}$, $\kappa = \alpha^3$, we find

$$u_4(x,t) = \frac{\alpha^2 A_1[\cosh(\alpha x - \frac{\alpha^3}{\gamma} t^{\gamma}) + \sinh(\alpha x - \frac{\alpha^3}{\gamma} t^{\gamma})]}{A_1 \cosh(\alpha x - \frac{\alpha^3}{\gamma} t^{\gamma}) + A_1 \sinh(\alpha x - \frac{\alpha^3}{\gamma} t^{\gamma}) + C_1 - \alpha^2 D_1}. \tag{21}$$

It is observed that the breath surfaces of (21) are presented in Figure 6.

Case 5. It is selected from the algorithm that when $D_1 = \frac{2C_1}{\alpha^2}$, $A_0 = -C_1$, $B_0 = 0$, $B_1 = \frac{A_1^2 - C_1^2}{\alpha^2 A_1}$, $\lambda = \frac{1}{\alpha}$, $\kappa = \alpha^3$. These coefficients produce

$$u_5(x,t) = \frac{\alpha^2 A_1}{A_1 + C_1 \cosh(\alpha x - \frac{\alpha^3}{\gamma} t^\gamma) + C_1 \sinh(\alpha x - \frac{\alpha^3}{\gamma} t^\gamma)}. \tag{22}$$

With the suitable values of parameters in (22), the graphs are plotted in Figure 7.

Case 6. If it is selected as $A_1 = -\frac{\sqrt{A_0 - \alpha^2 B_0}\sqrt{A_0^2 - C_1^2}}{\sqrt{A_0}}$, $D_1 = \frac{B_0 C_1}{A_0}$, $\kappa = -\frac{\alpha^3}{2} + \frac{3\alpha A_0}{2B_0}$, $\lambda = -\frac{\sqrt{B_0}\sqrt{3A_0 + \alpha^2 B_0}}{2A_0}$, $B_1 = \frac{-A_0^{\frac{5}{2}} B_0 \sqrt{A_0 - \alpha^2 B_0}\sqrt{A_0^2 - C_1^2} + \sqrt{\alpha^4 A_0^3 B_0^4 (A_0 - \alpha^2 B_1)(A_0^2 - C_1^2)}}{A_0^3 (A_0 - \alpha^2 B_0)}$, we have

$$u_6(x,t) = \frac{A_0 - \frac{\sqrt{A_0 - \alpha^2 B_0}\sqrt{A_0^2 - C_1^2}}{\sqrt{A_0}} \mathrm{sech}[\alpha x - \frac{\kappa}{\gamma} t^\gamma] + C_1 \tanh(\alpha x - \frac{\kappa}{\gamma} t^\gamma)}{\frac{\mathrm{sech}(\alpha x - \frac{\kappa}{\gamma} t^\gamma)\vartheta}{A_0^3 (A_0 - \alpha^2 B_0)} + B_0 [1 - \frac{\mathrm{sech}(\alpha x - \frac{\kappa}{\gamma} t^\gamma)\sqrt{A_0^2 - C_1^2}}{\sqrt{A_0}\sqrt{A_0 - \alpha^2 B_0}} + \frac{C_1 \tanh(\alpha x - \frac{\kappa}{\gamma} t^\gamma)}{A_0}]}, \tag{23}$$

where $\vartheta = \sqrt{\alpha^4 A_0^3 B_0^4 (A_0 - \alpha^2 B_0)(A_0^2 - C_1^2)}$ and $A_0 - \alpha^2 B_0 > 0$ for valid solution.

Case 7. Taking $D_1 = \frac{C_1(-A_0^2 + A_1^2 + C_1^2)}{\alpha^2(-A_0^2 + C_1^2)}$, $\lambda = -\frac{1}{2}\sqrt{\frac{(4A_0^2 - A_1^2 - 4C_1^2)(A_0^2 - A_1^2 - C_1^2)}{\alpha^2 (A_0^2 - C_1^2)^2}}$, $B_0 = \frac{A_0(A_0^2 - A_1^2 - C_1^2)}{\alpha^2 (A_0^1 - C_1^2)}$, $B_1 = \frac{(-A_0^2 + A_1^2 + C_1^2)(-2A_0^2 + A_1^2 + 2C_1^2)}{\alpha^2 A_1 (A_0^2 - C_1^2)}$, $\kappa = \alpha^3 - \frac{3\alpha^3 A_1^2}{2(-A_0^2 + A_1^2 + C_1^2)}$ gives the other breath solution

$$u_7(x,t) = \frac{\alpha^2 A_1 (\cosh(\alpha x - \frac{\kappa}{\gamma} t^\gamma) A_0 + A_1 + \sinh(\alpha x - \frac{\kappa}{\gamma} t^\gamma) C_1)(A_0^2 - C_1^2)}{\theta(-2A_0^2 - \cosh(\alpha x - \frac{\kappa}{\gamma} t^\gamma) A_0 A_1 + A_1^2 - \sinh(\alpha x - \frac{\kappa}{\gamma} t^\gamma) A_1 C_1 + 2C_1^2)}, \tag{24}$$

where $\theta = -A_0^2 + A_1^2 + C_1^2$. Figures 8 and 9 present some simulations of (24).

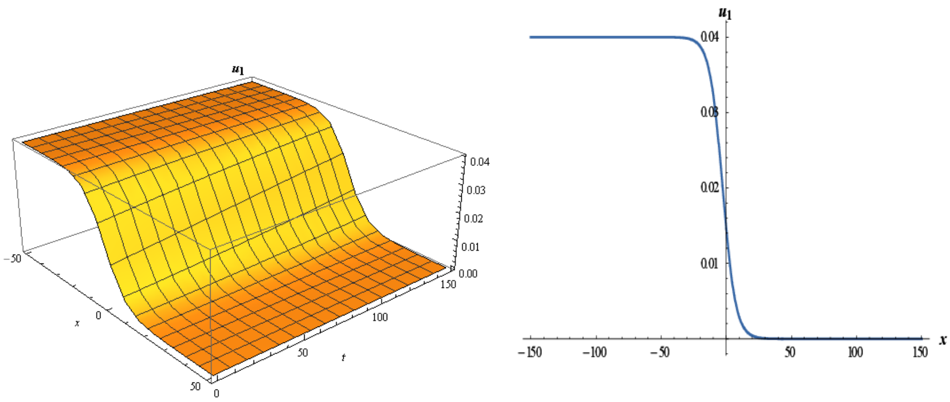

Figure 1. Three and two-dimensional surfaces of (18).

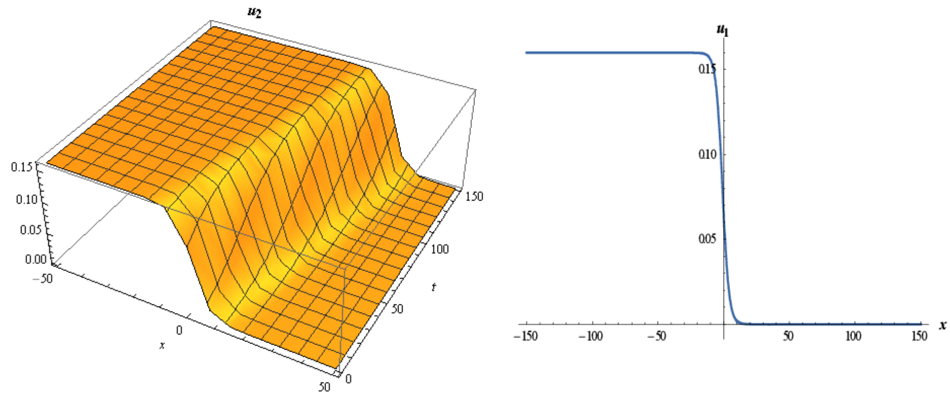

Figure 2. Three and two-dimensional surfaces of (19).

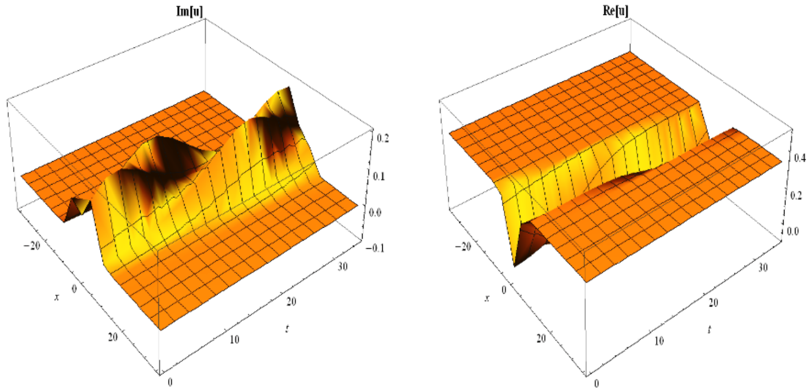

Figure 3. Three-dimensional graphs of imaginary and real part of (20).

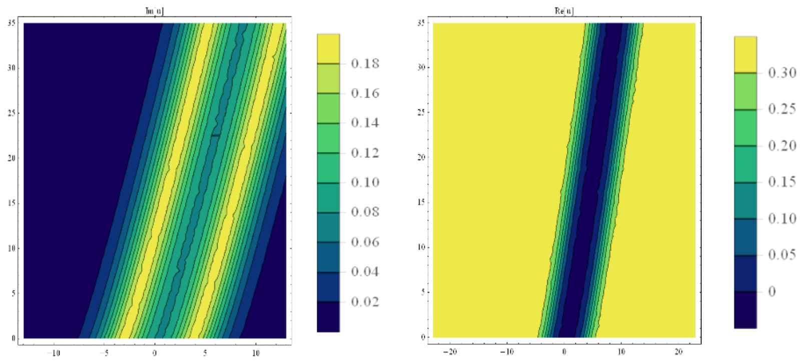

Figure 4. Contour graphs of imaginary and real part of (20).

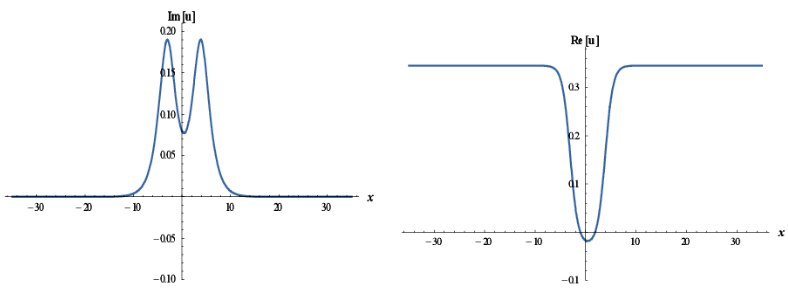

Figure 5. Two-dimensional graphs of imaginary and real part of (20).

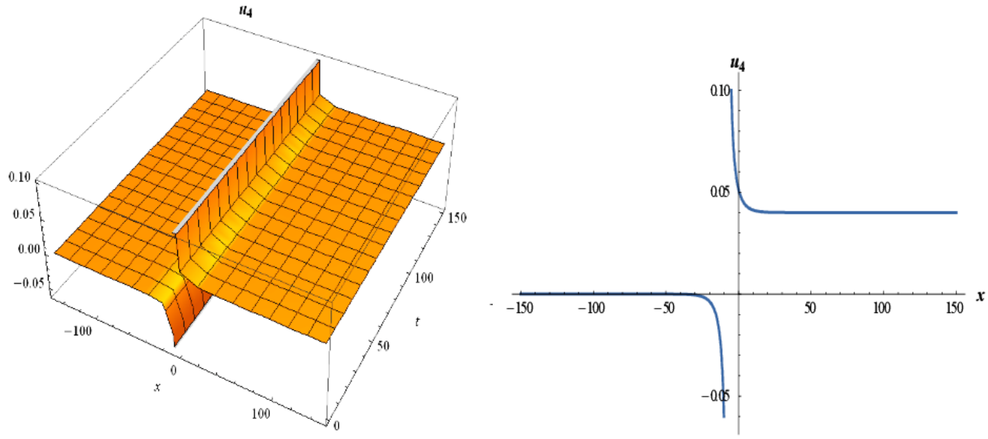

Figure 6. Three and two-dimensional surfaces of (21).

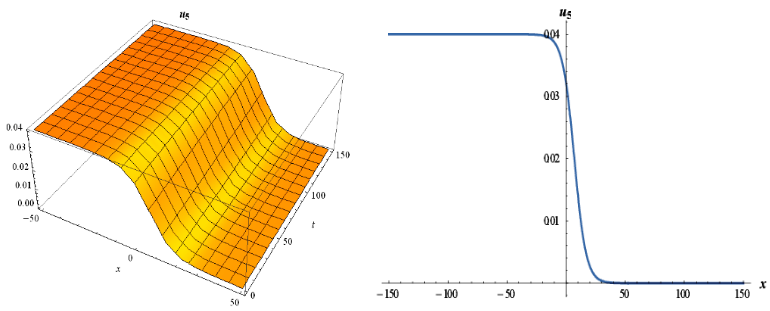

,

Figure 7. Three and two-dimensional surfaces of (22).

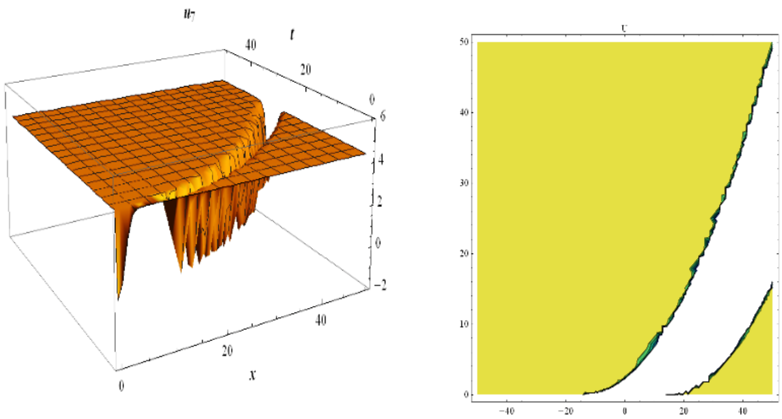

Figure 8. Three-dimensional and contour surfaces of (24).

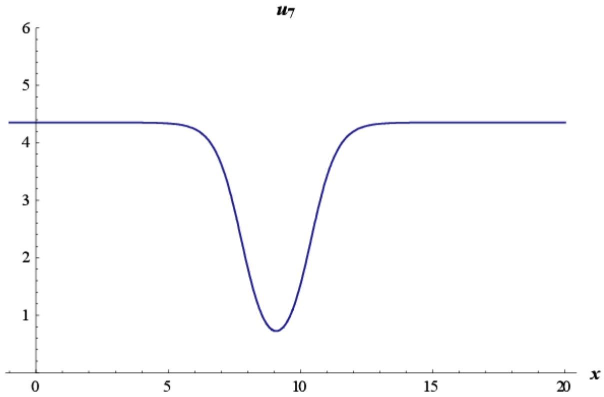

Figure 9. Two-dimensional surface of (24).

4.2. RSGEM for the mKdV-ZK Model with Conformable

This part applies RSGEM to the Equation (2) to extract some traveling wave solutions. The wave transformation formula is defined as

$$u(x,y,z,t) = U(\xi),\ \xi = \alpha x + \beta y + \theta z - \frac{k}{\gamma} t^{\gamma}, \tag{25}$$

where α, β, θ, k are nonzero real numbers and $0 < \gamma \leq 1$. Putting Equation (25) into Equation (2), the following NODE is obtained:

$$-kU' + \frac{p\alpha}{3}(U^3)' + (\alpha^3 + \alpha\beta^3 + \alpha\theta^2)U''' = 0. \tag{26}$$

Integrating (26) twice with respect to ξ and getting to the zero for both integral constants, we obtain

$$-3kU + p\alpha U^3 + 3(\alpha^3 + \alpha\beta^2 + \alpha\theta^2)U'' = 0. \tag{27}$$

Specially, if we take $n = m = 1$, we have

$$U(w) = \frac{A_1 sin(w) + C_1 cos(w) + A_0}{B_1 sin(w) + D_1 cos(w) + B_0}. \tag{28}$$

By substituting (28) into (27), we find the following solutions of (2).

Case 1. Considering $A_1 = -\frac{iC_1\sqrt{B_0^2 - B_1^2 - D_1^2}}{B_0}$, $A_0 = \frac{C_1 D_1}{B_0}$, $p = \frac{3kB_0^2}{\alpha C_1^2}$, $\theta = \frac{\sqrt{-2k - \alpha(\alpha^2+\beta^2)}}{\sqrt{\alpha}}$, we find

$$u_1 = \frac{C_1\left(D_1 - i\mathrm{sech}(\alpha x + \beta y - \frac{k}{\gamma}t^{\gamma} + \theta z)\sqrt{B_0^2 - B_1^2 - D_1^2} + B_0\tanh(\alpha x + \beta y - \frac{k}{\gamma}t^{\gamma} + \theta z)\right)}{B_0\left(B_0 + \mathrm{sech}(\alpha x + \beta y - \frac{k}{\gamma}t^{\gamma} + \theta z)B_1 + D_1\tanh(\alpha x + \beta y - \frac{k}{\gamma}t^{\gamma} + \theta z)\right)}, \tag{29}$$

where $B_0^2 - B_1^2 - D_1^2 > 0$ for a valid solution. Taking some values of parameters under the strain conditions, we plot its surfaces in Figures 10–12.

Case 2. If $A_1 = iC_1,\ B_1 = iD_1,\ A_0 = \frac{C_1 D_1}{B_0},\ p = \frac{3kB_0^2}{\alpha C_1^2},\ \theta = \frac{\sqrt{-2k-\alpha(\alpha^2+\beta^2)}}{\sqrt{\alpha}}$, we obtain

$$u_2 = \frac{C_1\left(D_1 + B_0(i\mathrm{sech}(\alpha x + \beta y - \frac{k}{\gamma}t^{\gamma} + \theta z) + \tanh(\alpha x + \beta y - \frac{k}{\gamma}t^{\gamma} + \theta z))\right)}{B_0\left(B_0 + D_1(i\mathrm{sech}(\alpha x + \beta y - \frac{k}{\gamma}t^{\gamma} + \theta z) + \tanh(\alpha x + \beta y - \frac{k}{\gamma}t^{\gamma} + \theta z))\right)}, \tag{30}$$

where $-2k - \alpha(\alpha^2 + \beta^2) > 0$ for a valid solution.

Case 3. If $A_0 = -\frac{A_1 D_1}{\sqrt{-B_0^2+B_1^2+D_1^2}}$, $C_1 = -\frac{A_1 B_0}{\sqrt{-B_0^2+B_1^2+D_1^2}}$, $p = -\frac{3(\alpha^2+\beta^2+\theta^2)(-B_0^2+B_1^2+D_1^2)}{2A_1^2}$, $k = -\frac{\alpha(\alpha^2+\beta^2+\theta^2)}{2}$, we extract

$$u_3 = \frac{A_1\Big(-\sinh(\alpha x+\beta y+\theta z+\frac{t^\gamma\alpha(\alpha^2+\beta^2\theta^2)}{2\gamma}\Big)B_0}{\Big(\cosh(\alpha x+\beta y+\theta z+\frac{t^\gamma\alpha(\alpha^2+\beta^2\theta^2)}{2\gamma})B_0+B_1+\sinh(\alpha x+\beta y+\theta z+\frac{t^\gamma\alpha(\alpha^2+\beta^2\theta^2)}{2\gamma})D_1\Big)\tau} - \frac{A_1\Big(\cosh(\alpha x+\beta y+\theta z+\frac{t^\gamma\alpha(\alpha^2+\beta^2\theta^2)}{2\gamma})D_1+\sqrt{-B_0^2+B_1^2+D_1^2}\Big)}{\Big(\cosh(\alpha x+\beta y+\theta z+\frac{t^\gamma\alpha(\alpha^2+\beta^2\theta^2)}{2\gamma})B_0+B_1+\sinh(\alpha x+\beta y+\theta z+\frac{t^\gamma\alpha(\alpha^2+\beta^2\theta^2)}{2\gamma})D_1\Big)\tau}, \tag{31}$$

where $\tau = \sqrt{-B_0^2+B_1^2+D_1^2}$, and also, $-B_0^2+B_1^2+D_1^2 > 0$ for a valid solution.

Case 4. In case of selecting $A_1 = 0,\ B_1 = 0,\ A_0 = \frac{C_1 D_1}{B_0},\ p = \frac{3kB_0^2}{\alpha C_1^2},\ \theta = \frac{\sqrt{-k-2\alpha(\alpha^2+\beta^2)}}{\sqrt{2}\sqrt{\alpha}}$, Equation (2) has the following hyperbolic function solution:

$$u_4 = \frac{C_1 D_1 + C_1 B_0 \tanh(\alpha x+\beta y-\frac{k}{\gamma}t^\gamma+\theta z)}{B_0^2 + B_0 D_1 \tanh(\alpha x+\beta y-\frac{k}{\gamma}t^\gamma+\theta z)}, \tag{32}$$

where $C_1 \neq 0, B_0 \neq 0, D_1 \neq 0$ for a valid solution.

Case 5. If we consider $A_1 = -\sqrt{A_0^2-C_1^2}, B_1 = 0, B_0 = \frac{C_1 D_1}{A_0}, p = -\frac{3(\alpha^2+\beta^2+\theta^2)D_1^2}{2A_0^2}$, $k = -\frac{\alpha(\alpha^2+\beta^2+\theta^2)}{2}$, we obtain

$$u_5 = \frac{A_0^2 - A_0 \operatorname{sech}(\alpha x+\beta y-\frac{kt^\gamma}{\gamma}+z\theta)\sqrt{A_0^2-C_1^2} + A_0 C_1 \tanh(\alpha x+\beta y-\frac{kt^\gamma}{\gamma}+z\theta)}{D_1 C_1 + D_1 A_0 \tanh(\alpha x+\beta y-\frac{kt^\gamma}{\gamma}+z\theta)D_1}, \tag{33}$$

where $A_0^2 - C_1^2 > 0$ for a valid solution.

Case 6. When $A_0 = -\frac{\sqrt{3}\sqrt{k}D_1}{\sqrt{p}\sqrt{\alpha}},\ A_1 = -\frac{i\sqrt{p\alpha C_1^2-3k(B_1^2+D_1^2)}}{\sqrt{p}\sqrt{\alpha}},\ B_0 = -\frac{\sqrt{p}\sqrt{\alpha}C_1}{\sqrt{3}\sqrt{k}},\ \beta = -\frac{\sqrt{-2k-\alpha(\alpha^2+\theta^2)}}{\sqrt{\alpha}}$, we find

$$u_6 = \frac{\Big(3\sqrt{k}(\sqrt{3}\sqrt{k}D_1 + i\operatorname{sech}(\alpha x-\frac{kt^\gamma}{\gamma}+\theta z-\Xi y)\omega - \sqrt{p}\sqrt{\alpha}C_1\tanh(\alpha x-\frac{kt^\gamma}{\gamma}+\theta z-\Xi y))\Big)}{\Big(\sqrt{3}p\alpha C_1 - 3\sqrt{3}\sqrt{k}\sqrt{p}\sqrt{\alpha}\operatorname{sech}(\alpha x-\frac{kt^\gamma}{\gamma}+\theta z-\Xi y)(B_1+\sinh(\alpha x-\frac{kt^\gamma}{\gamma}+\theta z-\Xi y)D_1)\Big)}, \tag{34}$$

where $\omega = \sqrt{p\alpha C_1^2 - 3k(B_1^2+D_1^2)}, \Xi = \frac{\sqrt{-2k-\alpha(\alpha^2+\theta^2)}}{\sqrt{\alpha}}$ for a valid solution. In Figures 13–15, several simulations are plotted.

Case 7. If $A_0 = \frac{\sqrt{3}\sqrt{k}D_1}{\sqrt{p}\sqrt{\alpha}},\ A_1 = iC_1,\ B_0 = \frac{\sqrt{p}\sqrt{\alpha}C_1}{\sqrt{3}\sqrt{k}},\ B_1 = iD_1,\ \beta = -\frac{\sqrt{-2k-\alpha(\alpha^2+\theta^2)}}{\sqrt{\alpha}}$ results in

$$u_7 = \frac{\frac{\sqrt{3}\sqrt{k}D_1}{\sqrt{p}\sqrt{\alpha}} + C_1\Big(i\operatorname{sech}(\alpha x-\frac{kt^\gamma}{\gamma}+\theta z-\Xi y)+\tanh(\alpha x-\frac{kt^\gamma}{\gamma}+\theta z-\Xi y)\Big)}{\frac{\sqrt{p}\sqrt{\alpha}C_1}{\sqrt{3}\sqrt{k}} + D_1\Big(i\operatorname{sech}(\alpha x-\frac{kt^\gamma}{\gamma}+\theta z-\Xi y)+\tanh(\alpha x-\frac{kt^\gamma}{\gamma}+\theta z-\Xi y)\Big)}, \tag{35}$$

where $\Xi = \frac{\sqrt{-2k-\alpha(\alpha^2+\theta^2)}}{\sqrt{\alpha}}$. Figures 16–18 present the graphs of (35).

Case 8. Coefficients such as $A_0 = \frac{\sqrt{3}\sqrt{k}D_1}{\sqrt{p}\sqrt{\alpha}}$, $A_1 = 0$, $B_0 = -\frac{\sqrt{p}\sqrt{\alpha}C_1}{\sqrt{3}\sqrt{k}}$, $B_1 = 0$, $\beta = -\frac{i\sqrt{k+2\alpha^3+2\alpha\theta^2}\sqrt{-p\alpha C_1^2+3kD_1^2}}{\sqrt{-2p\alpha^2C_1^2+6k\alpha D_1^2}}$ produce

$$u_8 = \frac{\frac{3\sqrt{3}\sqrt{k}D_1}{\sqrt{p}\sqrt{\alpha}} - 3\sqrt{k}C_1\tanh(\alpha x - \frac{kt^\gamma}{\gamma} + \theta z - \frac{iy\sqrt{k+2\alpha^3+2\alpha\theta^2}\sqrt{-p\alpha C_1^2+3kD_1^2}}{\sqrt{-2p\alpha^2C_1^2+6k\alpha D_1^2}})}{\sqrt{3}\sqrt{p}\sqrt{\alpha}C_1 - 3\sqrt{k}D_1\tanh(\alpha x - \frac{kt^\gamma}{\gamma} + \theta z - \frac{iy\sqrt{k+2\alpha^3+2\alpha\theta^2}\sqrt{-p\alpha C_1^2+3kD_1^2}}{\sqrt{-2p\alpha^2C_1^2+6k\alpha D_1^2}})}. \tag{36}$$

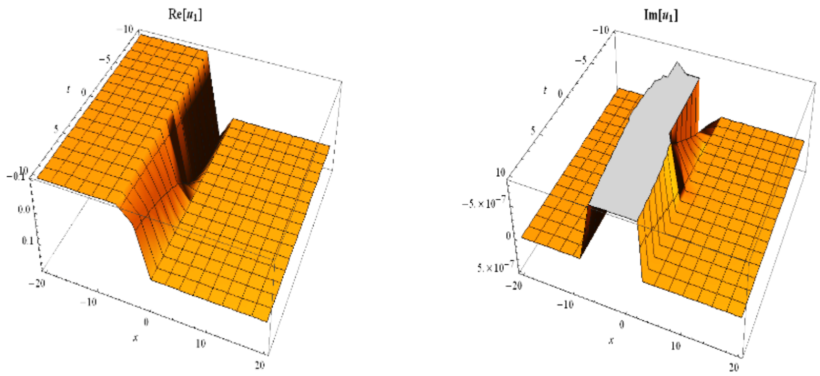

Figure 10. Three-dimensional graphs of imaginary and real part of (29).

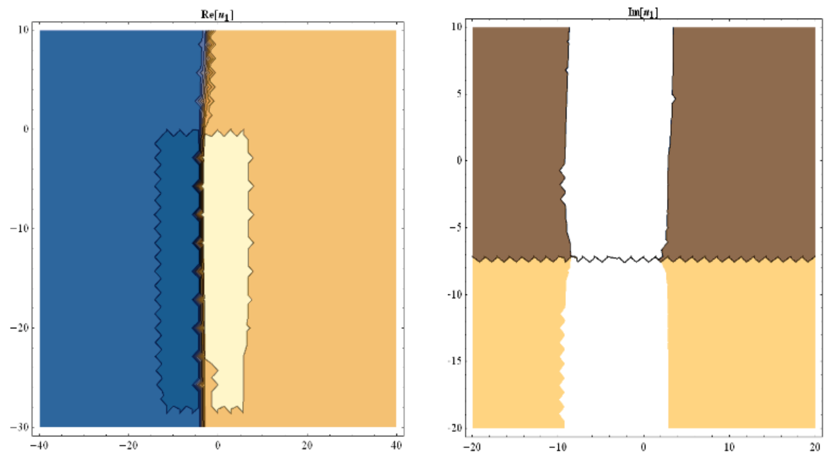

Figure 11. Contour graphs of imaginary and real part of (29).

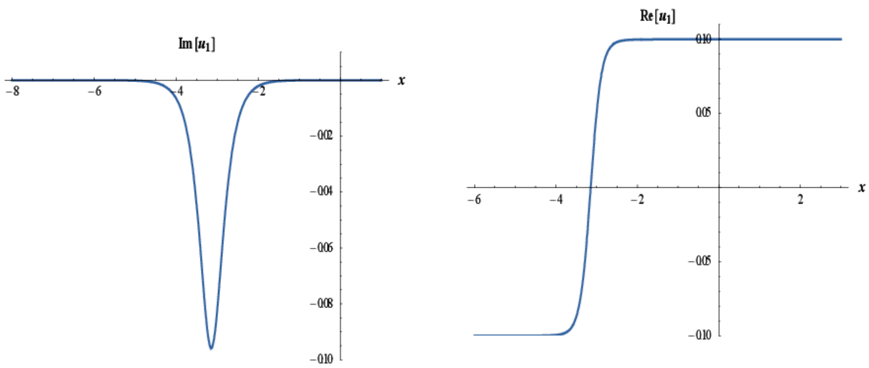

Figure 12. Two-dimensional graphs of imaginary and real part of (29).

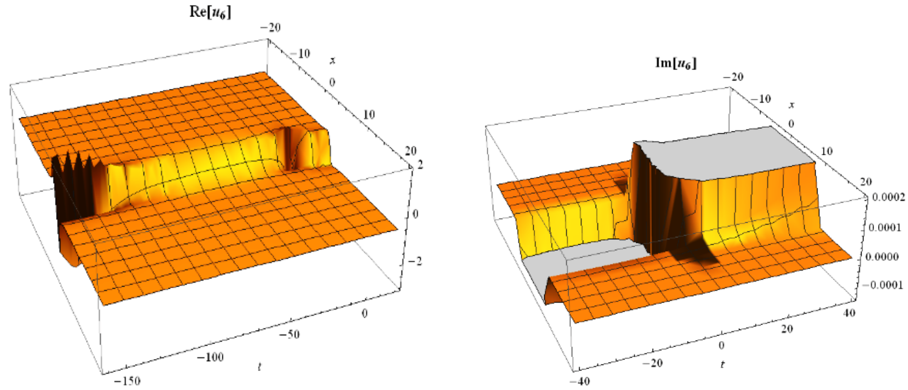

Figure 13. Three-dimensional graphs of imaginary and real part of (34).

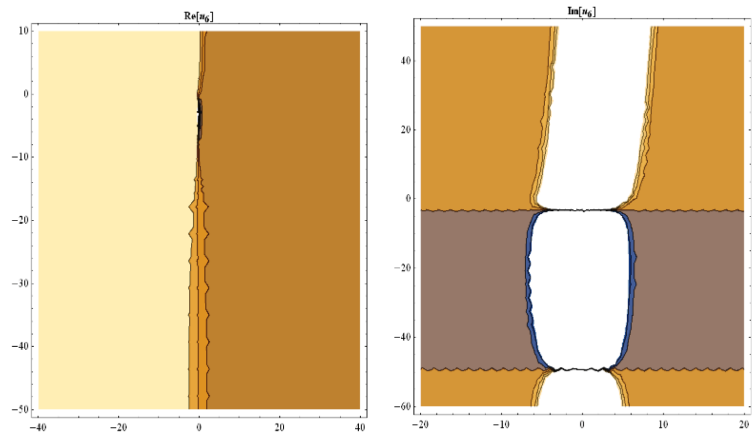

Figure 14. Contour graphs of imaginary and real part of (34).

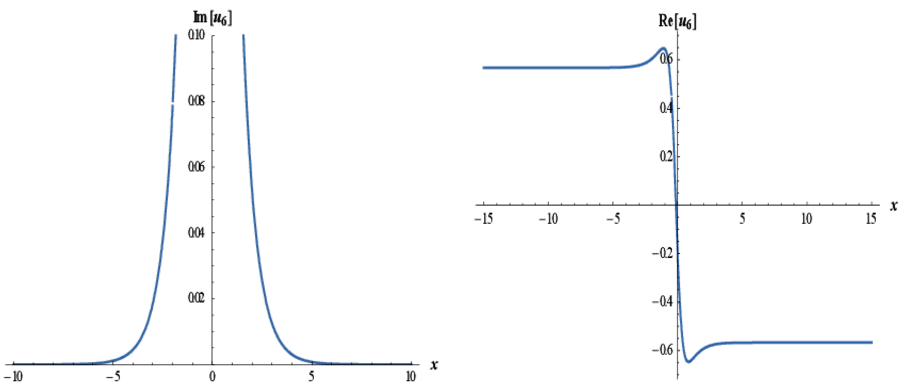

Figure 15. Two-dimensional graphs of imaginary and real part of (34).

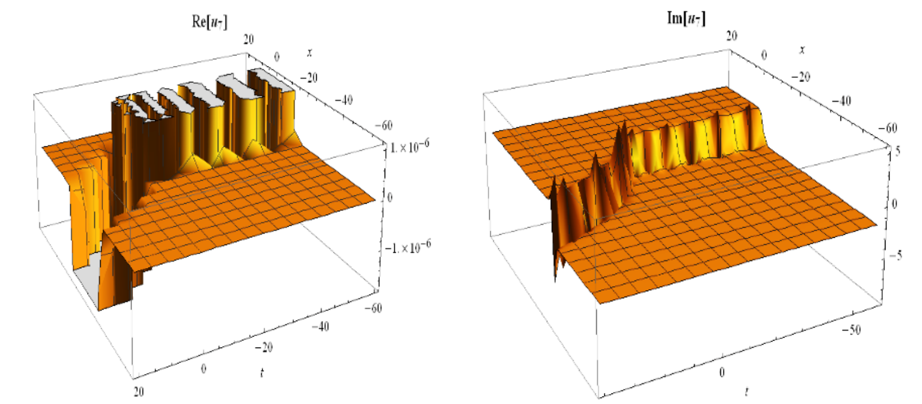

Figure 16. Three-dimensional graphs of imaginary and real part of (35).

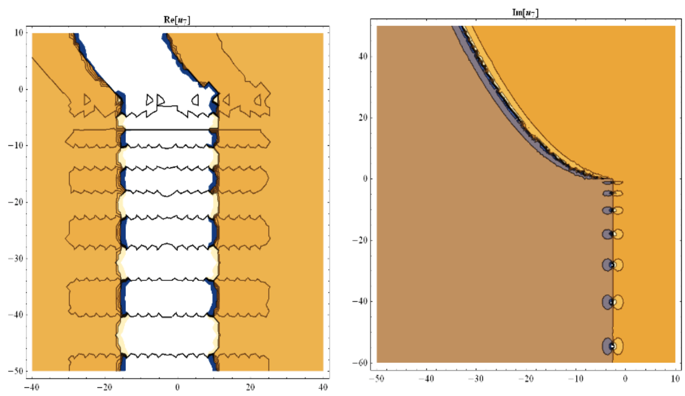

Figure 17. Contour graphs of imaginary and real part of (35).

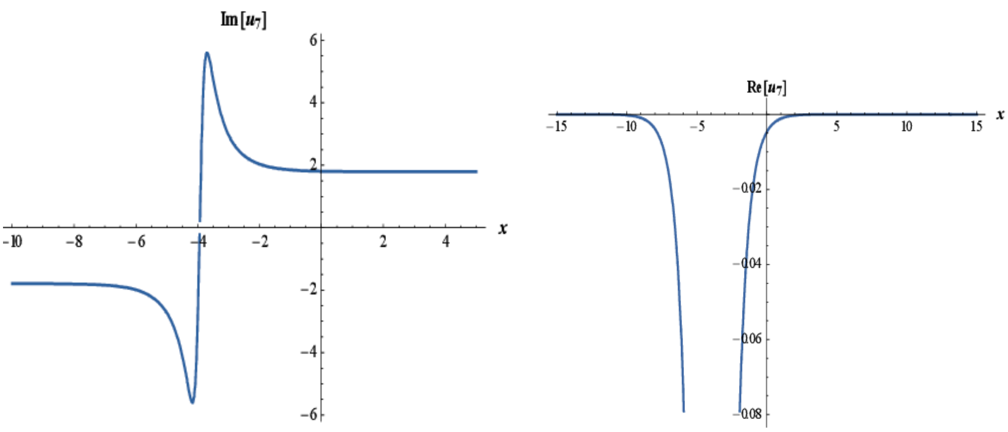

Figure 18. Two-dimensional graphs of imaginary and real part of (35).

5. Discussion and Physical Meanings

By using RSGEM, we found some traveling wave solutions of the nonlinear Gardner and (3+1)-dimensional mKdV-ZK equations including a conformable operator. These solutions are in the forms of the rational, hyperbolic, periodic, trigonometric, complex and mixed hyperbolic function solutions. Figure 1 symbolizes the exponential surfaces of (18) when $D_1 = 1.5$, $\alpha = 0.2, C_1 = -0.5, A_1 = 0.32, \gamma = 0.99, -50 < x < 50$, $0 < t < 150$ for 3D and $t = 0.21$ for 2D. Figure 2 represents the hyperbolic function graphs of (19) when $D_1 = 1.5$, $\alpha = 0.2, C_1 = -0.5, \gamma = 0.99, -50 < x < 50, 0 < t < 150$ for 3D and $-150 < x < 150, t = 0.21$ for 2D. Figure 3 explains the 3D graphs in $-35 < x < 35, 0 < t < 35$, and Figure 4 investigates the 2D with $-13 < x < 13, t = 0.1$. Figure 5 represents the contour surfaces with $0 < t < 35$ of the complex hyperbolic function solution of (20) if it is selected as $D_1 = 0.5, \alpha = -0.65, C_1 = 0.1, B_0 = 2, \gamma = 0.99, \kappa = -0.2$. Figure 6 presents the 3D and 2D graphs of the hyperbolic function solution of (21) for $D_1 = 1.5, \alpha = 0.2, C_1 = 0.5$, $A_1 = -2, \gamma = 0.5, t = 0.5, -150 < x < 150$, for 3D and $0 < t < 150$, $-150 < x < 150$ for 2D solutions. Figure 7 is used to explain the 3D and 2D hyperbolic function solution of (22) for $\alpha = 0.2, C_1 = 0.5, A_1 = 2, \gamma = 0.99, 0 < t < 150 - 50 < x < 50$, for 3D and $t = 0.12 - 150 < x < 150$ for 2D solutions. Figures 8 and 9 symbolize the singular wave distributions of (24) under the $\alpha = 2$, $A_0 = 7, C_1 = -0.2, A_0 = 2, \gamma = 0.5, 0 < x < 50$, $50 < t < 50, -50 < x < 50, 0 < t < 50$, and $t = 1$ for 2D. Figures 10–12 are plotted to observe the 3D, 2D and contour surfaces of the mixed hyperbolic function solution of (29) under $C_1 = 0.3, D_1 = 0.12, B_0 = 3, \alpha = 4, \beta = 3, \gamma = 0.5, k = 0.3, z = 1.5, y = 2.5$, $\theta = 3.4, B_1 = 0.13, -20 < x < 20, -10 < t < 10$ for 3D and $t = 0.01$ for 2D solutions. Figures 13–15 are plotted to explain 3D, 2D and contour surfaces of the mixed complex hyperbolic function solution (34) under the terms of $C_1 = 0.3, D_1 = 0.12$, $\alpha = 1.4$, $\gamma = 0.5$, $k = 0.3, z = 1.5, y = 2.5, \theta = 1.4, A_0 = 1.3, p = 2, B_1 = 1.2, -20 < x < 20, -160 < t < 20$, $-20 < x < 20, -40 < t < 40$ for 3D, and, $-40 < x < 40, -50 < t < 10, -20 < x < 20$ for contour graph and $t = 0.2 \ -10 < x < 10$, $-15 < x < 15$ for 2D graph. Figures 16–18 introduce the singular wave properties of (35) under the values of $C_1 = 0.2, D_1 = 0.12$, $\alpha = 1.4, \gamma = 0.5, k = -3, z = 1.5, y = 2.5, \theta = 1.4, p = 2, -60 < x < 20$, $-60 < t < 20$, for 3D graphs and $-40 < x < 40, -50 < t < 10, -60 < t < 50$ for the contour surface, as well as $t = 0.1$, $-15 < x < 15$ for the 2D graph.

6. Conclusions

In this paper, we have successfully applied RSGEM to the nonlinear Gardner and (3+1)-dimensional mKdV-ZK equations including a conformable operator. We extracted some solutions such as complex, rational, exponential, complex hyperbolic and mixed complex function solutions. We have chosen suitable values of the parameters, and some graphical simulations are also plotted. Necessary strain conditions are also reported in detail. When we consider these results and Figures 1–18, it may be observed that these solutions are used to explain the wave distributions for the governing models. Moreover, it is observed that these findings produce the estimated behaviors of models. When we compare these solutions with [38], it may be seen that these are new wave function solutions.

In this paper, we considered $n = m = 1$ in particular. If we consider other equalities of n and m, this will produce more sophisticated solutions to the models studied. This newly presented method can be also used to find many entirely new traveling, singular and complex solutions to the nonlinear partial differential equations arising in real-world problems.

Author Contributions: Conceptualization, L.Y.; methodology, G.Y.; validation, A.K.; formal analysis, W.G.; writing—original draft preparation, A.K.; Supervision, H.M.B. All authors have read and agreed to the published version of the manuscript.

Funding: This research received no external funding.

Institutional Review Board Statement: Not applicable.

Informed Consent Statement: Not applicable.

Data Availability Statement: Not applicable.

Acknowledgments: Authors want to extend their thanks to editors and anonymous referees for their valuable effort on developing our paper.

Conflicts of Interest: The authors declare no conflict of interest.

References

1. Debnath, L. Recent applications of fractional calculus to science and engineering. *Int. J. Math. Math. Sci.* **2003**, *2003*, 3413–3442. [CrossRef]
2. Hilfer, R. *Applications of Fractional Calculus in Physics*; World Scientific Pub Co Pte Ltd.: Munich, Germany, 2000.
3. Lakshmikantham, V.; Vatsala, A. Basic theory of fractional differential equations. *Nonlinear Anal. Theory Methods Appl.* **2008**, *69*, 2677–2682. [CrossRef]
4. Raynaud, H.-F.; Zergainoh, A. State-space representation for fractional order controllers. *Automatica* **2000**, *36*, 1017–1021. [CrossRef]
5. Podlubny, I. *Fractional Differential Equations, Mathematics in Science and Engineering*; Academic Press: San Diego, CA, USA, 1999.
6. Sabatier, J.; Agrawal, O.P.; Machado, J.A.T. *Advances in Fractional Calculus*; Springer: Dordrecht, The Netherlands, 2007.
7. Khalil, R.; Al Horani, M.; Yousef, A.; Sababheh, M. A new definition of fractional derivative. *J. Comput. Appl. Math.* **2014**, *264*, 65–70. [CrossRef]
8. Abdeljawad, T. On conformable fractional calculus. *J. Comput. Appl. Math.* **2015**, *279*, 57–66. [CrossRef]
9. Brzeziński, D.W. Comparison of Fractional Order Derivatives Computational Accuracy—Right Hand vs Left Hand Definition. *Appl. Math. Nonlinear Sci.* **2017**, *2*, 237–248. [CrossRef]
10. Youssef, I.K.; El Dewaik, M.H. Solving Poisson's Equations with fractional order using Haarwavelet. *Appl. Math. Nonlinear Sci.* **2017**, *2*, 271–284. [CrossRef]
11. Eslami, M.; Rezazadeh, H. The first integral method for Wu–Zhang system with conformable time-fractional derivative. *Calcolo* **2016**, *53*, 475–485. [CrossRef]
12. Khan, M.A.; Hammouch, Z.; Baleanu, D. Modeling the dynamics of hepatitis E via the Caputo–Fabrizio derivative. *Math. Model. Nat. Phenom.* **2019**, *14*, 311. [CrossRef]
13. Rezazadeh, H.; Tariq, H.; Eslami, M.; Mirzazadeh, M.; Zhou, Q. New exact solutions of nonlinear conformable time-fractional Phi-4 equation. *Chin. J. Phys.* **2018**, *56*, 2805–2816. [CrossRef]
14. Osman, M.S.; Korkmaz, A.; Rezazadeh, H.; Mirzazadeh, M.; Eslami, M.; Zhou, Q. The unified method for conformable time fractional Schroodinger equation with perturbation terms. *Chin. J. Phys.* **2018**, *56*, 2500–2506. [CrossRef]
15. Feng, Q. A new approach for seeking coefficient function solutions of conformable fractional partial differential equations based on the Jacobi elliptic equation. *Chin. J. Phys.* **2018**, *56*, 2817–2828. [CrossRef]
16. Yokuş, A.; Gülbahar, S. Numerical Solutions with Linearization Techniques of the Fractional Harry Dym Equation. *Appl. Math. Nonlinear Sci.* **2019**, *4*, 35–42. [CrossRef]
17. Cattani, C. A Review on Harmonic Wavelets and Their Fractional Extension. *J. Adv. Eng. Comput.* **2018**, *2*, 224–238. [CrossRef]
18. Cattani, C.; Srivastava, H.M.; Yang, X.J. *Fractional Dynamics*; De Gruyter: Berlin, Germany, 2015; pp. 1–5.
19. Veeresha, P.; Ilhan, E.; Prakasha, D.G.; Baskonus, H.M.; Gao, W. A new numerical investigation of fractional order susceptible-infected-recovered epidemic model of childhood disease. *Alex. Eng. J.* **2022**, *61*, 1747–1756. [CrossRef]
20. Kumar, D.; Singh, J.; Baleanu, D. Sushila Analysis of regularized long-wave equation associated with a new fractional operator with Mittag-Leffler type kernel. *Phys. A Stat. Mech. Its Appl.* **2018**, *492*, 155–167. [CrossRef]
21. Ravichandran, C.; Logeswari, K.; Jarad, F. New results on existence in the framework of Atangana–Baleanu derivative for fractional integro-differential equations. *Chaos Solitons Fractals* **2019**, *125*, 194–200. [CrossRef]
22. Baskonus, H.M.; Cattani, C.; Ciancio, A. Periodic Complex and Kink-type Solitons for the Nonlinear Model in Microtubules. *J. Appl. Sci.* **2019**, *21*, 34–45.
23. Ravichandran, C.; Jothimani, K.; Baskonus, H.M.; Valliammal, N. New results on nondensely characterized integrodifferential equations with fractional order. *Eur. Phys. J. Plus* **2018**, *133*, 109. [CrossRef]
24. Dananea, J.; Allalia, K.; Hammouch, Z. Mathematical analysis of a fractional differential model of HBV infection with antibody immune response. *Chaos Soliton Fractals* **2020**, *136*, 109787. [CrossRef]
25. Gao, W.; Yel, G.; Baskonus, H.M.; Cattani, C. Complex solitons in the conformable (2 + 1)-dimensional Ablowitz-Kaup-Newell-Segur equation. *AIMS Math.* **2020**, *5*, 507–521. [CrossRef]
26. Ganji, R.; Jafari, H.; Baleanu, D. A new approach for solving multi variable orders differential equations with Mittag–Leffler kernel. *Chaos Solitons Fractals* **2020**, *130*, 109405. [CrossRef]
27. Sadeghi, S.; Jafari, H.; Nemati, S. Operational matrix for Atangana–Baleanu derivative based on Genocchi polynomials for solving FDEs. *Chaos Solitons Fractals* **2020**, *135*, 109736. [CrossRef]
28. Singh, J.; Kumar, D.; Hammouch, Z.; Atangana, A. A fractional epidemiological model for computer viruses pertaining to a new fractional derivative. *Appl. Math. Comput.* **2018**, *316*, 504–515. [CrossRef]
29. Rahaman, H.; Hasan, M.K.; Ali, A.; Alam, M.S. Implicit Methods for Numerical Solution of Singular Initial Value Problems. *Appl. Math. Nonlinear Sci.* **2021**, *6*, 1–8. [CrossRef]
30. Gao, W.; Ismael, H.F.; Husien, A.M.; Bulut, H.; Baskonus, H.M. Optical Soliton solutions of the nonlinear Schrödinger and resonant nonlinear Schrödinger equation with parabolic law. *Appl. Sci.* **2020**, *10*, 219. [CrossRef]
31. Ismael, H.F.; Bulut, H.; Baskonus, H.M. Optical soliton solutions to the Fokas–Lenells equation via sine-Gordon expansion method and (m+(G′/G))(m+(G′/G))-expansion method. *Pramana* **2020**, *94*, 35. [CrossRef]
32. Bulut, H.; Ilhan, E. Fractional vector-borne disease model with lifelong immunity under Caputo operator. *Phys. Scr.* **2021**, *96*, 084006. [CrossRef]

33. Prakasha, D.G.; Veeresha, P.; Baskonus, H.M. Two novel computational techniques for fractional Gardner and Cahn-Hilliard equations. *Comput. Math. Methods* **2019**, *1*, e1021. [CrossRef]
34. Alderremy, A.; Saad, K.M.; Agarwal, P.; Aly, S.; Jain, S. Certain new models of the multi space-fractional Gardner equation. *Phys. A Stat. Mech. Its Appl.* **2020**, *545*, 123806. [CrossRef]
35. Iyiola, O.S.; Olayinka, O.G. Analytical solutions of time-fractional models for homogeneous Gardner equation and non-homogeneous differential equations. *Ain Shams Eng. J.* **2014**, *5*, 999–1004. [CrossRef]
36. Cao, D. The classification of the single traveling wave solutions to the time-fraction Gardner equation. *Chin. J. Phys.* **2019**, *59*, 379–392. [CrossRef]
37. Pandir, Y.; Duzgun, H.H. New Exact Solutions of Time Fractional Gardner Equation by Using New Version of F -Expansion Method. *Commun. Theor. Phys.* **2017**, *67*, 9. [CrossRef]
38. Yel, G.; Sulaiman, T.A.; Baskonus, H.M. On the complex solutions to the (3 + 1)-dimensional conformable fractional modified KdV-Zakharov-Kuznetsov equation. *Mod. Phys. Lett. B* **2020**, *34*, 2050069, . [CrossRef]
39. Baskonus, H.M.; Guirao, J.L.G.; Kumar, A.; Causanilles, F.S.V.; Bermudez, G.R. Complex mixed dark-bright wave patterns to the modified α and modified Vakhnenko-Parkes equations. *Alex. Eng. J.* **2020**, *59*, 2149–2160. [CrossRef]
40. Guirao, J.L.G.; Baskonus, H.M.; Kumar, A. Regarding New Wave Patterns of the Newly Extended Nonlinear (2+1)-Dimensional Boussinesq Equation with Fourth Order. *Mathematics* **2020**, *8*, 341. [CrossRef]
41. Baskonus, H.M. New acoustic wave behaviors to the Davey–Stewartson equation with power-law nonlinearity arising in fluid dynamics. *Nonlinear Dyn.* **2016**, *86*, 177–183. [CrossRef]
42. Yamgoue, S.B.; Deffo, G.R.; Pelap, F.B. A new rational sine-Gordon expansion method and its application to nonlinear wave equations arising in mathematical physics. *Eur. Phys. J. Plus* **2019**, *134*. [CrossRef]